

Synthesis and Characterization of Graphene/Polythiophene (GR/PT) Nanocomposites: Evaluation as High-Performance Supercapacitor Electrodes

J. P. Melo¹, E. N. Schulz^{2, 3}, C. Morales-Verdejo¹, S. L. Horswell³, M. B. Camarada^{1,*}

¹ Universidad Bernardo OHiggins, Centro de Biología y Química Integrativa (CIBQA), General Gana 1702, Santiago, Chile

² Instituto de Ingeniería Electroquímica y Corrosión, INIEC-CONICET, Universidad Nacional del Sur, Av. Alem 1253, Bahía Blanca, 8000, Argentina.

³ School of Chemistry, University of Birmingham, Edgbaston, Birmingham, B15 2TT, United Kingdom.

*E-mail: maria.camarada@ubo.cl

Received: 19 December 2016 / Accepted: 1 February 2017 / Published: 12 March 2017

Composites of polythiophene (PT) and graphene (GR) with different mass proportions were studied for their application as supercapacitors. Fourier transform infrared spectroscopy (FTIR) along with High Resolution Scanning electron microscopy (HR-SEM) were employed in order to characterize the morphology and composition of the resulting composites. The electrochemical behaviour of these composites was studied by means of cyclic voltammetry and specific capacitance curves were derived from these measurements. The Faradaic impedance spectroscopy response of the different composites, along with that of GR, was also studied. From these measurements it was found that a 1:1 in mass composite of GR and PT showed a higher specific capacitance, even when compared with GR alone. The introduction of the GR in that proportion also showed an enhanced cyclic stability in comparison with the sole polymer. The high specific capacitance (365 F g^{-1} at 1 A g^{-1}) of this composite material indicates its potential for use as an electrode material for supercapacitors.

Keywords: Graphene, polythiophene, nanocomposites, supercapacitors

1. INTRODUCTION

Modern society's energy needs often exceed the current production capabilities. Added to this problem, the rapid worldwide depletion of fossil-fuel resources demands the pursuit of more sustainable energy alternatives, including both renewable energy sources and sustainable storage

technologies [1]. It is for these reasons that research efforts are currently being focused on the development of more efficient energy storage and delivery systems. Recent studies on energy storage materials, have placed electrochemical supercapacitors as promising energy storage solutions [2-4]. These devices offer important advantages when compared with conventional energy storage media, such as batteries and conventional capacitors, providing superior energy densities and power while having a longer life cycle [5,6]. Supercapacitors can be classified into two general categories: electrical double layer capacitors (EDLCs) and pseudo capacitors (PCs). EDLCs store electrical energy by using the electrical double layer capacitance through an electrostatic charge storage mechanism. In contrast, PCs are related to the fast reversible faradaic reactions at the surface of electroactive materials [7,8]. The main characteristics of EDLCs are a high charge accumulation, usually associated with the large exposed surface area, a good conductivity, along with a low production cost and a long life cycle [9]. However, their energy density and specific capacitance are similar to those of a conventional capacitor. On the other hand, PCs display a high energy density and a fast loss of power density at the cost of a shorter life cycle [10]. PCs can store a greater charge than EDLCs because of the smaller charge separation at the electrode/electrolyte interface and the pseudocapacitance resulting from faradaic reactions at the electrode/electrolyte interface. Nevertheless, the use of PCs is usually restricted to low working voltages. They also show stability issues and unsatisfactory high-rate capabilities, arising from low conductivities of electrode materials [11].

Many carbon materials, such as activated carbon, mesoporous carbon, carbon nanotubes, and graphene (GR) have been employed for EDLCs because of their high surface area. Among these compounds GR, a single layer of sp^2 -bonded carbon atoms, is among the most attractive materials because of its excellent electrical and thermal conductivity, electrochemical stability and mechanical properties [12,13]. In the case of PCs, different conducting polymers [14,15] such as polyaniline (PANI) [16], polypyrrole (PPy) [17] and polythiophene (PT) [18] have been employed as electrode materials. However, they often suffer from low electrical conductivities, inherent rigidity and structural degradation, leading to low power density and poor charge/discharge stability.

During the last years, efforts have been focused on the improvement of the energy density of supercapacitors and the preservation of their high power capability while improving the length of their life cycle [19-21]. With this aim, GR was proposed as an appropriate frame to support pseudo-capacitive materials such as conducting polymers, because of its mechanical flexibility, large surface area and high electrical conductivity. The synergistic effect of these high capacitance materials along with flexibility that GR provides, results in an active electrode material with a better performance than other available alternatives. Additionally, GR-based supercapacitors usually exhibit a high specific capacitance ($135\text{--}264\text{ F g}^{-1}$) [22-24]. Many studies have referred to the preparation of composites of GR with conducting polymers through classical polymerization methodologies and electropolymerization. The resulting materials usually show better electrochemical properties than their pure conducting polymer counterparts, such as a higher conductivity and increased stability during the charge/discharge process [25,26]. Among the materials synthesized by *in situ* polymerization, PANI composites have caught the attention of researchers because of their low cost, environmental stability and facile synthesis. Yan *et al.* reported a GR/PANI composite with a specific capacitance of 489 F g^{-1} at 0.4 A g^{-1} [27]. In the case of PPy, Liu *et al.* have reported a series of

GR/PPy composites obtained through classical polymerization, achieving a maximum specific capacitance of 650 F g^{-1} at 0.45 A g^{-1} current density, with an excellent cycling stability and a 95% of the specific capacitance retained after 5000 cycles [28]. In the literature, one can find several studies related to the use of PANI and PPy composites with GR. However, to this date, not many reports have been directed to the systematic study of the properties of polythiophene and graphene composites [29].

PT is considered as one of the most promising CPs because of its low cost, high environmental stability and good electrical conductivity, among other specific properties. Laforgue and co-workers performed the first known study using PT as a supercapacitor. In their work they reported a specific storage level of 110 F g^{-1} [18]. Since then, several compounds, such as carbon nanotubes and metal oxides, have been employed to improve the properties of PT [30,31]. In this way, it was shown that a noticeable improvement on the thermal and electrical conductivities of the PT composite was achieved, when compared to that of pure PT. Zhao *et al.* have synthesized an electromagnetic material using GR nanosheet/PT composites prepared using the traditional chemical polymerization method. The composites exhibited a clear hysteretic behaviour and characteristics of a semiconductor, although the authors did not characterize electrochemically their use in energy storage applications [32]. A study published in 2011 explored the use of a GR/PT composite as supercapacitor [33], reporting a specific capacitance derived from cyclic voltammograms of 176 F g^{-1} at 50 mV s^{-1} . Nonetheless, no reports about electrochemical characterization of composites with different ratios of GR and PT have been written up to this date, to the best of our knowledge. In this work, traditional chemical polymerization was applied to synthesize a series of GR/PT composites with different compositions, in order to characterize the influence of this factor on the final properties of the compound when employed as a supercapacitor. The supercapacitor performances of the resulting materials were tested and compared with each other. The specific capacitance of the best composite can reach 365 F g^{-1} at a discharge current density of 1 A g^{-1} , which is much larger than the value achieved using pure PT (92 F g^{-1}). The mixture, when prepared with certain ratios of GR and conducting PT, may open the opportunity to prepare low-cost, high performance electrode materials for supercapacitor applications.

2. EXPERIMENTAL

2.1. Reagents

Reagents were of analytical grade or the highest commercially available purity and were used as received. Graphite, KCl, $\text{K}_3[\text{Fe}(\text{CN})_6]$ and $\text{K}_4[\text{Fe}(\text{CN})_6]$ were purchased from Merck. Thiophene monomer was purchased from Sigma Aldrich. Solutions used in electrochemical measurements were prepared with ultrapure water of resistivity not less than $18 \text{ M}\Omega \text{ cm}$ (Milli-Q, USA).

2.2. Synthesis of graphene oxide (GO) and reduced graphene oxide (GR)

Graphene oxide was prepared *via* Hummers' method with some modifications [34]. Briefly, 4 g of graphite powder were dissolved with vigorous stirring in 10 mL of H_2SO_4 at 90°C and oxidized

using a combination of powerful reagents: 2 g of $K_2S_2O_8$ and 2 g of P_2O_5 . The stirring continued for four more hours at a temperature of 80 °C. The solution was then diluted with 500 mL of Milli-Q water. After dilution, the solution was stirred overnight. The pre-oxidized graphite was then filtered and washed with deionized water until a neutral pH was achieved, and then dried at room temperature overnight. This powder was then subjected to further oxidation with 92 mL of H_2SO_4 and 12 g of potassium permanganate ($KMnO_4$) in an ice bath solution. The mixture was stirred for 2 more hours at 35 °C. After this, 184 mL of Milli-Q water was added to the mixture. The reaction was terminated by the addition of 10 mL of H_2O_2 and 560 mL of Milli-Q water to reduce the manganese in the solution. The colour of the mixture changed to a bright yellow and the mixture was then stirred overnight. The precipitate was centrifuged at 3000 rpm and washed with water until reaching a neutral pH. Finally, the obtained GO was filtered and dried under vacuum at 40°C for 24 h, to avoid decomposition (GO deoxygenates above 60 to 80 °C). Chemical conversion of GO to reduced graphene oxide (GR) was completed according to a reported method [35]: 2 g of GO were dispersed in 1000 mL of water. Then 2.5 mL of hydrazine monohydrate were added and the mixture was heated at 95 °C during 1 h. Finally, the GR was collected by filtration. The resulting product, a black powder, was washed several times with Milli-Q water to remove the excess hydrazine and was dried in a vacuum oven at 30 °C.

2.3. Synthesis of graphene/polythiophene (GR/PT) nanocomposites and PT

The preparation of the composites was based on the methodology reported by Zhao *et al.* with slight modifications [32]. Briefly, 0.2 g of GR were added to 50 mL chloroform and thoroughly mixed. Later, 8.0 g of the oxidizing agent $FeCl_3$ were added into the mixture and stirred for 30 min. 1.0 g of thiophene monomer was added to the solution and left under agitation for 12 h at 5 °C. Then the solution was filtered and washed with Milli-Q water. The precipitate was re-suspended in 100 mL of 1 M HCl and stirred for 2 h. After filtration, the solid was rinsed with a 1 M HCl solution until the filtrate was colourless. Following the rinsing, the composite was then washed with Milli-Q water until a pH 7 was reached. The GR/PT composites were then dried under vacuum conditions at a temperature of 40 °C for 24 h. Following the procedures described above, different ratios of GR were mixed with PT in the following mass proportions: 0.5:1, 1:1 and 2:1. For the sake of simplicity, the resulting compounds will be represented in relation to the mass percentage of PT in the following manner: GR/PT-67, -50 and -33, respectively. The synthesis of PT consisted of mixing two previous stirred solutions: 1.0 g thiophene in 10 mL of chloroform and 8.0 g of the oxidizing agent $FeCl_3$ in 50 mL of chloroform. The mixture was stirred during 12 h at temperature of 5 °C. After the filtration and washing, the solid was re-suspended and washed using the same procedure applied for the GR/PT composites. The PT solid was dried under vacuum at 60 °C for 24 h.

2.4. Characterization Methods

Fourier transform infrared spectroscopy (FTIR) spectra were measured using a Jasco FT/IR 4100 spectrometer in the frequency range 500 – 4000 cm^{-1} , on preparing a KBr pellet. UV-visible

spectra were recorded with a Jasco V-630 UV-visible spectrophotometer. All measurements were taken at room temperature. High Resolution Scanning electron microscopy (HR-SEM) was carried out using a FEI equipment model INSPECT- F50.

2.5. Electrochemical measurements

A CH Instruments (CHI 760E) potentiostat/galvanostat electrochemical workstation was used to measure the electrochemical properties of the samples at ambient temperature (20 °C). A conventional three-compartment cell was employed throughout the work. A glassy carbon electrode (GCE, 0.07 cm² geometric area) was used as a working electrode. The counter electrode was a coiled Pt wire of large area, separated from the electrolytic solution by a sintered glass frit. Prior to each experiment, the working electrode was polished to a mirror finish with an aqueous alumina slurry (particle size 0.3 and 0.05 micron) on micro-cloth pads, rinsed thoroughly with water, ultra-sonicated for 5 min in Milli-Q water and dried. Before performing the surface modification, cyclic voltammetry (CV) was performed on the GCE in the potential range from -0.2 to +0.6 V in 5 mM K₃[Fe(CN)₆] solution until reproducible cyclic voltammograms (CVs) were obtained. All potentials quoted are referred to a Ag/AgCl/KCl (1 M) electrode. Each working solution was purged with high purity argon for 15 min prior to each experiment and the flow was maintained over the solution during the measurements. The modified working electrodes were prepared by dissolving the active material in N,N-dimethylformamide (DMF) (1 mg mL⁻¹) with ultra-sonication for 1 h, in order to get a homogenous suspension. Then, 5 μL of the suspension were dropped onto the cleaned electrode and dried at RT for 12 h. CV and galvanostatic charge-discharge measurements were carried out in 1 M KCl at scan rates ranging from 10 to 100 mV s⁻¹ within a potential range of -0.2 to 0.6 V, while electrochemical impedance spectroscopy (EIS) was performed at AC voltage amplitude of 0.01 V and a frequency range from 0.1 to 1000 kHz at open circuit potential, in a solution containing 5 mM K₃[Fe(CN)₆], 5mM K₄[Fe(CN)₆] and 0.1 M KCl.

3. RESULTS AND DISCUSSION

3.1. GO, GR and GR/PT characterization

The FT-IR spectra of graphite, GO, GR, PT and GR/PT composites are shown in Figure 1. In the case of GO, the spectrum revealed oxygen functionalities at 3400 (O-H stretching vibrations), 1728 (C=O stretching vibrations) and 1054 cm⁻¹ (C-O stretching vibrations), confirming the effective oxidation of graphite to GO. At 1622 cm⁻¹ appeared C=C skeletal vibrations from un-oxidized graphitic diamonds (Figure 1a). The spectrum of pure graphite had broad absorption bands at 3440 and 1040 cm⁻¹ corresponding to the O-H and C-O stretching vibrations respectively [36]. The absorption peak at 1640 cm⁻¹ was attributed to the skeletal vibrations of C=C [37]. The GO spectrum is quite different from that of graphite (which contains few oxygen-containing functional groups), confirming the successful oxidation of the graphite.

In the case of Figure 1b, GR presents a peak related to the O-H stretching vibrations at 3400 cm^{-1} which was significantly reduced in comparison with GO as a result of the deoxygenation process [38]. The characteristic signal of the skeletal vibration of GR is at about 1560 cm^{-1} [39-41]. The peak at 1403 cm^{-1} can be attributed to O-H deformation vibrations of tertiary C-OH [42], while the band at 1113 cm^{-1} can be assigned to the C-O stretching vibration [43,44].

The characteristic peaks of PT are at $1640, 1400, 1212, 1030, 780, 690$ and 470 cm^{-1} . The peaks at 1640 and 1400 cm^{-1} correspond to the C=C asymmetric and symmetric stretching vibrations of the thiophene ring, respectively [45,46]. The band at 1212 cm^{-1} was related to C-C stretching vibrations. The C-H in-plane bending band is at 1030 cm^{-1} [47]. The band at 780 cm^{-1} belongs to the C-H out-of-plane vibration of the 2,5-substituted thiophene monomer [48], while the peaks at 690 cm^{-1} and 470 cm^{-1} are related to the C-S stretching in the thiophene ring [30,49-51] and the C-S-C ring deformation [52], respectively.

In the case of the GR/PT composites (Figure 1b) the spectra contain a mixture of the GR and PT characteristic absorption bands. Some peaks assigned to PT are slightly shifted, such as the C-C vibration at 1203 cm^{-1} , the C-H in-plane bending band at 1028 cm^{-1} and the C-S stretching in the thiophene ring at 690 cm^{-1} . These signal displacements indicate that the GR is interacting in some way with PT. Furthermore, there is a new absorption peak at 1323 cm^{-1} , mainly present in GR/PT-50 and 67 (the composites with higher amount of PT), which confirms that there may be new atomic vibrations related to the synthesized materials.

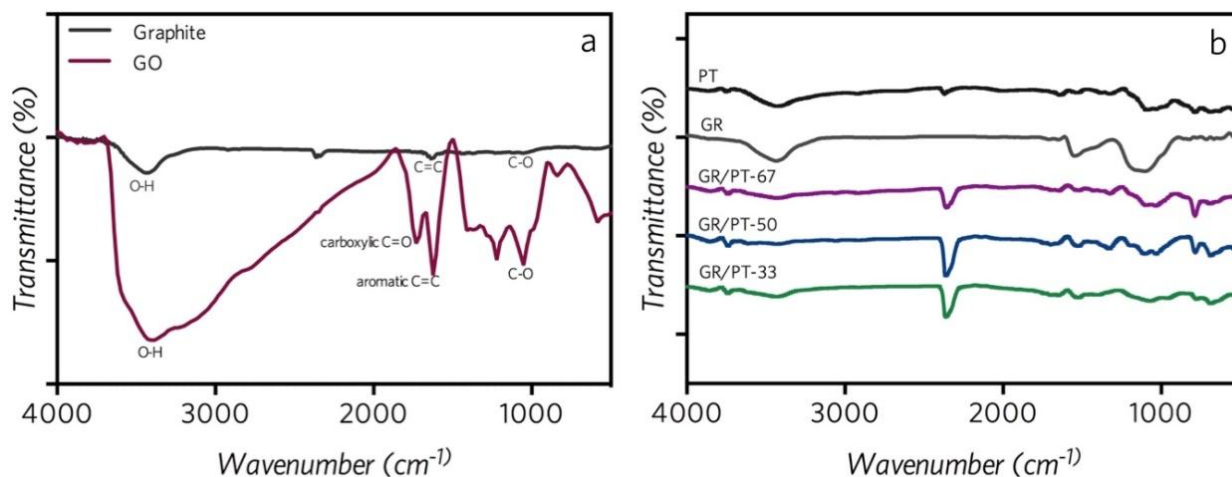


Figure 1. FTIR spectra of (a) graphite and GO and (b) GR, PT and the composites. All spectra were taken with a KBr pellet.

UV-visible spectra of the samples were also measured. As Figure 2 shows, the UV-vis spectrum of the GO solution ($0.1\text{ mg}\cdot\text{mL}^{-1}$ in water) shows two bands: a maximum at 237 nm , which can be assigned to the π/π^* transition of aromatic C-C bonds, and a shoulder at approximately 315 nm corresponding to n/π^* transition of the C=O bonds. After reduction of GO with hydrazine, GR (0.1 mg mL^{-1} in methanol) exhibits its characteristic band at 270 nm . This bathochromic shifting of the

band indicates that the electronic conjugation within the reduced graphene was recovered upon reduction of the graphene oxide [38].

The PT profile (0.1 mg mL^{-1} in THF), shows a strong band at 370 nm which is attributed to the π/π^* transition of the 2,5-thiophenylene unit. An additional broad band appears at around 544 nm which is related to the bipolaron state of PT [53]. The GR/PT spectrum ($0.1 \text{ mg}\cdot\text{mL}^{-1}$ in THF) exhibited peaks associated with PT, the GR/PT-67 being the one with highest peaks related to the bigger PT content.

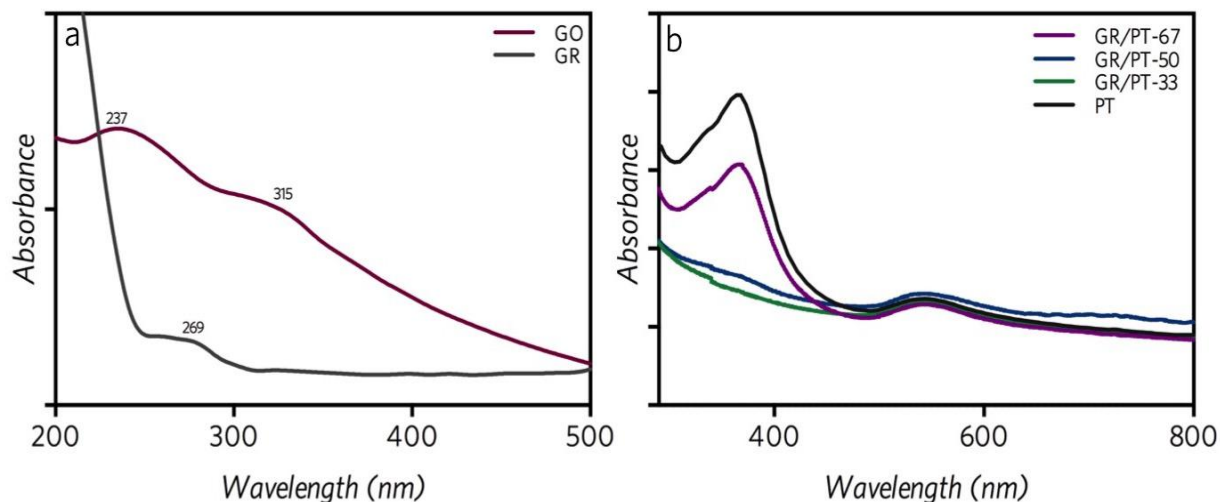


Figure 2. UV-visible spectra of (a) GO and GR, and (b) PT and the GR/PT composites.

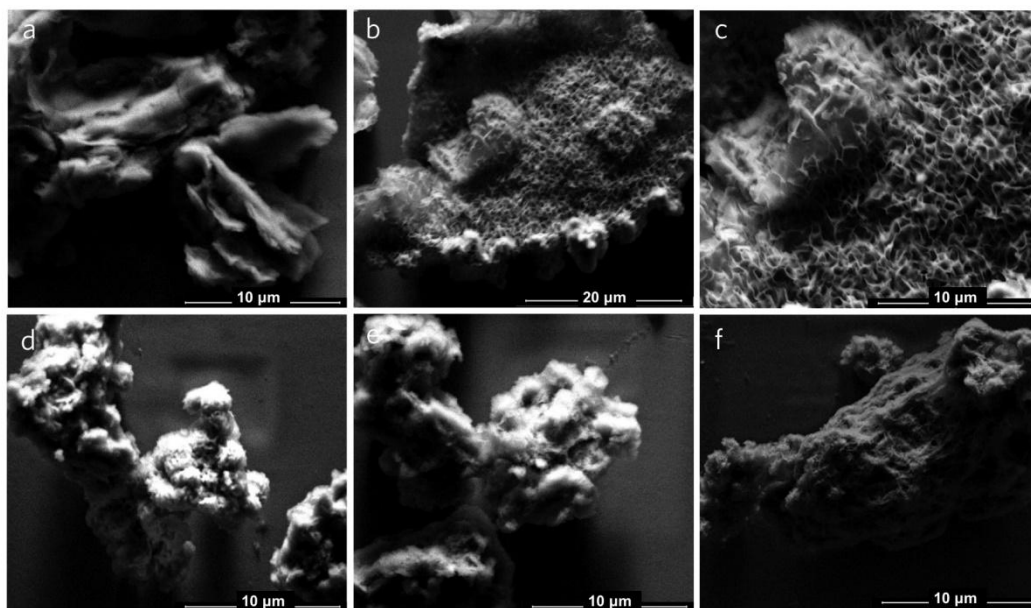


Figure 3. SEM images of (a) GR, (b) PT ($20 \mu\text{m}$), (c) PT ($10 \mu\text{m}$) and the composites GR/PT (d) -67, (e) -50 and (f) -33.

All samples were also characterized using HR-SEM. The surface morphologies of the GR, PT and PT/GR composites are shown in Figure 3. The GR presents a multi-layered sheet structure, while the PT images show a granular and uniform structure, with a repetitive pattern. In the case of the GR-PT composites, the uniform morphology of PT vanishes and a mixture of coarse and flaky structure is observed. As long as the percentage of PT in the composites decreases, the structure shows a greater number of lineal layers, as can be seen in GR/PT-33 structure (Figure 3f), related to the higher amount of GR in the composite.

In all the GR/PT images, the PT granular structures are decorating the surface of the GR sheets, indicating the formation of PT chains on the surface of the GR. The different structures present in the GR/PT composites from GR and PT, demonstrates the formation of new materials.

3.2. Electrochemical behaviour

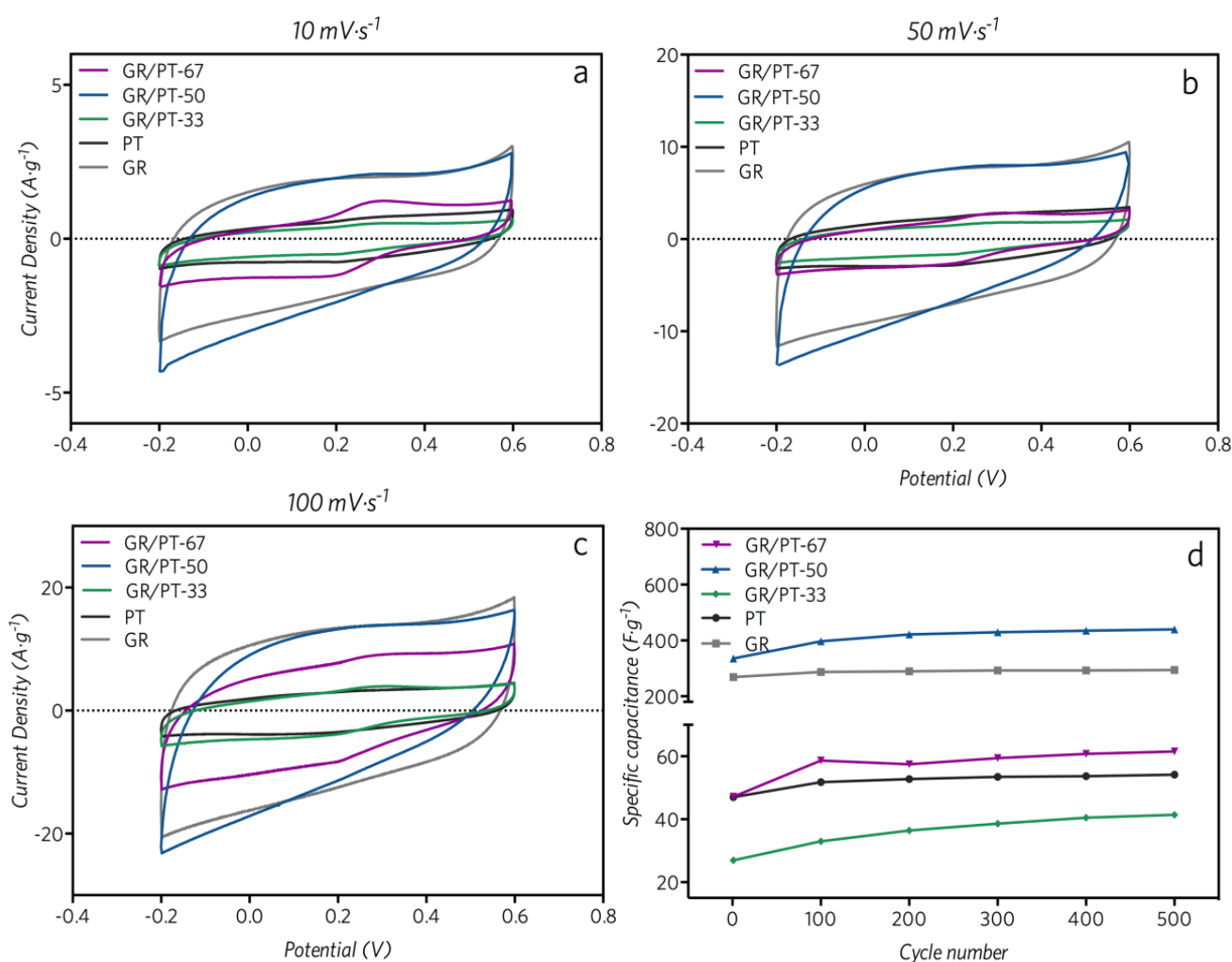


Figure 4. CVs of the synthesized compounds in KCl 1 M for a potential window of -0.2 and 0.6 V (vs Ag/AgCl KCl 1 M) at a scan rate of (a) 10, (b) 50 and (c) 100 mV s⁻¹, and (d) specific capacitance of the films from the 1st to the 500th cycle at a scan rate of 50 mV s⁻¹.

The electrochemical performance of the samples when employed as an electrode material for supercapacitors was tested by cyclic voltammetry (CV) and the galvanostatic charge–discharge technique in a three-electrode electrochemical system. Figure 4 displays the CVs of each of the synthesized materials deposited on a GCE electrode. A rectangular shape of the CVs is expected in the case of an ideal double layer capacitance.

The CVs obtained for the PT, GR/PT-67 and -33 electrodes exhibited a nearly rectangle shape with small redox peaks. These peaks are due to the oxidation (0.3 V) and reduction of the PT (0.2 V). In the case of GR/PT-67 these peaks were higher in current density when compared with those of the unmodified PT film.

This is probably related to a greater conductivity of the material owing to the presence of GR, although GR/PT-67 presented lower current densities than those of pure GR. The GR/PT-33 enclosed area is smaller than that of PT, showing a much lower capacitance. This is probably related to the loss of conjugation of the GR due to the presence of PT. The shapes of the GR and GR/PT-50 curves show the rectangular symmetric current–potential characteristics, which are typical of an ideal capacitive behaviour. In addition, it has also been observed for both cases that there are no clear redox peaks in the potential range studied. The rectangular shape remained even at a higher scan rate of 100 mV s^{-1} , which is indicative of a highly capacitive nature with a good ion response. It is also observed that the redox current increased with the increase in the scan rate, indicating a good rate capability. The rectangular shape of the CV curve of GR/PT-50 was larger than that of PT, suggesting a larger capacitance than that of the latter. Therefore, the presence of GR sheets in the GR/PT-50 composite may largely reduce the conductive resistance, leading to the observed enhanced capacitive behaviour when compared with that of PT. Specific capacitances derived from cyclic voltammetry experiments were calculated by means of the following equation [7]:

$$C = \left(\int i dV \right) / \nu m V$$

where C (F g^{-1}) is the specific capacitance, m (g) is the mass of active materials loaded on the working electrode, ν (V s^{-1}) is the scan rate, i (A) is the current and V (V) is the potential window of the CV tests. Figure 4d shows the cyclic stability of the synthesized materials at a scan rate of 50 mV s^{-1} after 500 cycles. The lowest specific capacitance is shown by GR/PT-33, followed by those of PT and GR/PT-67. This indicates that the ratio of PT to GR in the composite is highly relevant for the final performance of the material as a supercapacitor. The GR/PT-33 composite showed a reduction of the general performance when compared with that of PT, and GR/PT-67 exhibited a small improvement over the latter, but below that of GR. This agrees with what was observed in the CV profiles, where low quantities of GR in the composite, as in the case of GR/PT-67, improved the behaviour of the material when compared with PT, but not with GR. Conversely, higher amounts of GR, like in the case of GR/PT-33, result in a much lower conductivity than that of PT or GR, probably because of the break of the conjugation effects of GR in the presence of PT. The GR/PT-50 composite displayed an enhancement of the specific capacitance over PT and showed better C values than those of GR. The introduction of the latter material enhanced the stability of the GR/PT-50 composite towards potential cycling. This is because GR can stabilize the structure of PT during the cycling process and improve its performance when compared with the sole polymer.

In all cases there is an increase in the C values after some voltammetric cycles, because of the higher resistance of the films. GR presents the lowest variation of specific capacitance after 500 cycles (9.5%) *i.e.* the best stability towards cycling, followed by PT with 15%. The GR/PT-67 and -50 composites exhibited the same variation (31%), while the GR/PT-33 showed the worst capacitance conservation, with an increase of 54%, which indicates that the material is destroyed after several cycles and therefore, is not a good candidate for a supercapacitor as a result of its low capacity retention.

Figure 5 shows the charge/discharge curves of the synthesized materials. All curves exhibit an almost equilateral triangular shape and the potential-time relationships are all approximately linear, indicating a good reversibility during the charge-discharge processes and good capacitive behaviour. From the specific capacitance curves it is clearly seen that there is an important difference in the behaviour between the composites, which is dependent on the ratio of GR to PT. Based on the charge/discharge curves, the specific capacitance (C) of a single electrode in a three electrode system can be calculated by applying the following equation [54,55]:

$$C = \frac{i \Delta t}{m \Delta V}$$

where i (A) is the discharge current, Δt (s) is the discharge time, m (g) is the mass of the active electrode material and ΔV (V) is the voltage range. The specific capacitances for the modified electrodes are summarized in Figure 5d. As expected, at a higher current density all the values of the specific capacitance for the materials studied decreased.

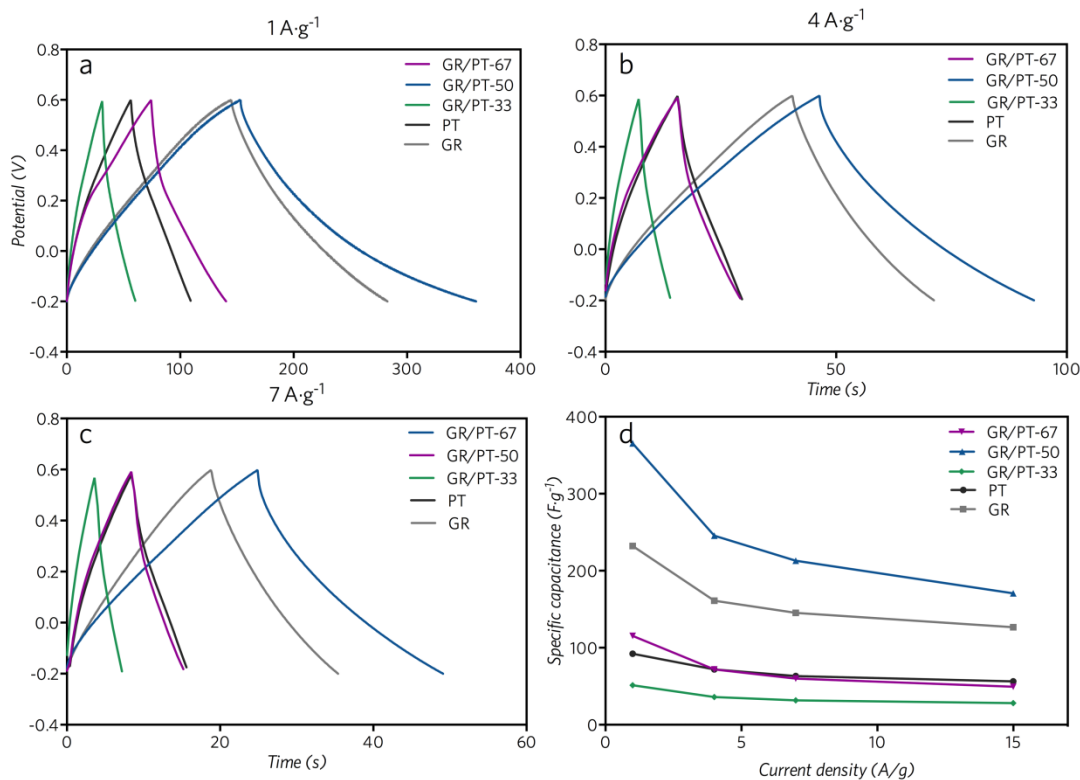


Figure 5. Charge/discharge curves of the synthesized materials at a current density of (a) 1, (b) 4 and (c) $7 \text{ A}\cdot\text{g}^{-1}$ and the specific capacitances of the electrodes at different current densities.

The specific capacitance of the GR/PT-50 composite is the highest observed among all of the samples, with a value of 365 F g^{-1} at current density of 1 A g^{-1} . This value exceeds that of the pure GR (232 F g^{-1}) and quadruples the value obtained for pure PT (92 F g^{-1}). PT, GR/PT-33 and GR/PT-67 showed the lowest C values, leaving the GR/PT-50 specific capacitance value as the highest reported to date for a PT and GR composite.

It is worth noting that the GR/PT-50 composite shows not only the highest capacitance, but also the best rate capability, indicating that the ratio between GR and PT is the optimum of all the samples studied. Higher amounts of PT in the composite, as in the case of GR/PT-67, do not retain the conductive properties of the GR. On the other hand, when small quantities of thiophene are polymerized, as in the case of GR/PT-33, the resulting composite loses the well-known capacitance characteristics of the GR. Based on the evidence above, the improved electrical double-layer capacitance and better rate capability of the GR/PT-50 composite might be mainly ascribed to the good pseudo-capacitance of the GR and a synergistic effect with PT, which can shorten the ion diffusion length. The higher specific capacitance obtained for the GR/PT-50 composite, when compared with that of GR, can be ascribed to the rapid insertion/extraction of doping ions, the increase in the effective surface area and a higher conductivity.

It is important to mention that the reported C values vary according to different experimental techniques and electrolytes. Table 1 summarizes capacitance values for different graphene-conducting polymers composites at different current densities.

Table 1. Experimental capacitance values of different graphene and conducting polymers based materials at different current densities.

Material	Synthesis method	C (F g^{-1})	Current density (A g^{-1})
GR [56]	Vacuum filtration	215	0.1
GR-PANI [27]	Polymerization	489	0.4
GR-PANI nanofibers [57]	Vacuum filtration	210	1
GR-PANI paper [58]	Electropolymerization	763	1
GR-PPy [28]	Polymerization	650	0.45
GR-PT [33]	Polymerization	176	-
GR-PEDOT [33]	Polymerization	374	0.01
PEDOT/PT-GO [57]	Polymerization	320	1
GR-PT derivative [59]	Polymerization	217	0.3

Under the same condition of a current density of 1 A g^{-1} and synthesis methodology applied in the present study, the specific capacitance measured from the charge-discharge curve of the GR/PT-50 composite showed a marked improvement over previously reported values for other conducting polymer composites based on PT, such as the PEDOT/PT-GO composite (320 F g^{-1}) [57] and GR-PT (176 F g^{-1}) [33]. However, this last study only reported C at different scan rates and not at a specific current density. GR/PT-50 has the best cyclability and specific capacitance retention of all the synthesized materials (365 F g^{-1}). The better performance might be attributed to the interlinked graphene sheets with the conjugated thiophene polymer which facilitates electron movements and at the same time, increases the electrode conductivity.

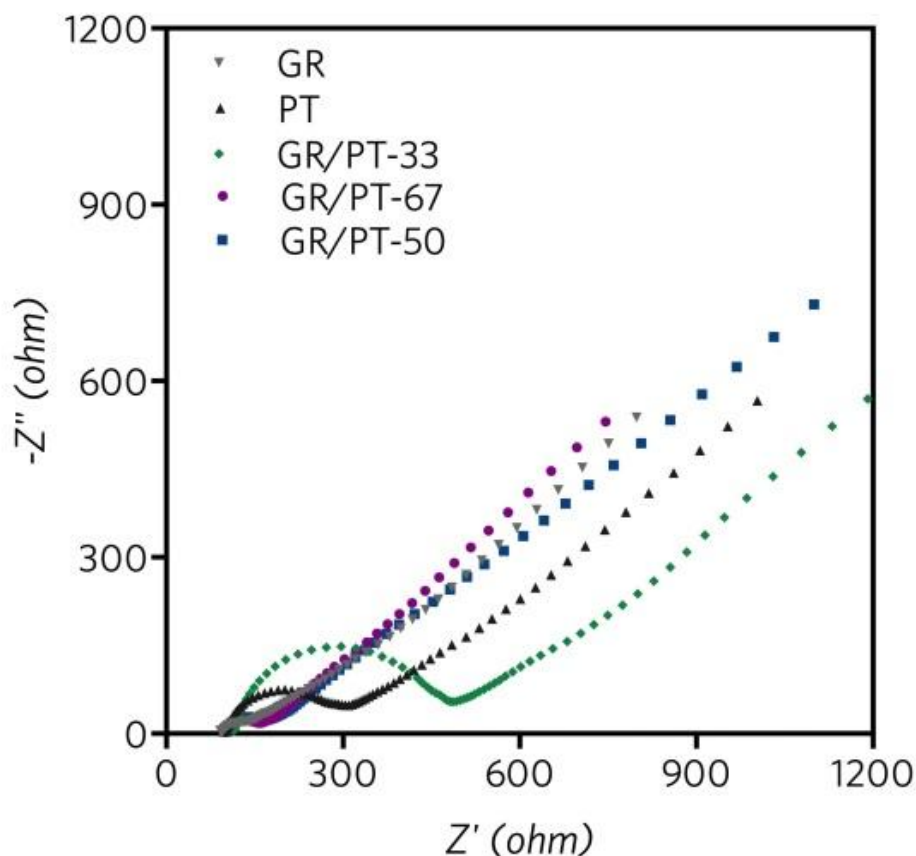


Figure 6. Nyquist plots of the modified electrodes at open circuit potential in 5 mM $\text{K}_3[\text{Fe}(\text{CN})_6]$, 5 mM $\text{K}_4[\text{Fe}(\text{CN})_6]$ and 0.1 M KCl.

These results are in agreement with previous reports about rapid ion transport in graphene sheets [60]. Moreover, the higher specific capacitance value in comparison to reported studies can be attributed to the specific amount of PT in the final composite, demonstrating that the mixing ratio between GR and PT is a key factor in the final performance of the material. Other conducting polymers, GR/PANI composite (489 F g^{-1}) [27] and GR-PPy (500 F g^{-1}) [58] provided faster electrochemical reaction indicating that the electrochemical performance of GR-PT supercapacitors should be further optimized.

With the aim of obtaining a deeper insight into the capacitance and other relevant electrochemical information of the composite materials studied, we performed a series of impedance spectroscopy experiments. The better conductivity of GR/PT-50 is further confirmed by the Nyquist plots. Figure 6 shows the electrochemical impedance spectra for the modified GCE electrode with the synthesized materials. Traditionally, an impedance plot can be divided into two parts: the high and the low-frequency regions. In the high-frequency zone, a semicircular shape was obtained in all cases, which is related to interfacial processes. The larger diameter of the arc for the PT and the GR/PT-33 modified GCE electrode indicates a low charge transfer rate resulting from a high electron transfer resistance. In the case of GR/PT-50 and -67, the semicircle is smaller, suggesting that the electron transfer resistance is lower. Then, the incorporation of GR into the PT polymer in certain proportions improves the conductive properties of the composite. At low frequencies, the imaginary part of the impedance spectra is related to the capacitive behaviour of the electrode and approaches a 90° vertical line in an ideal capacitor. The 45°-sloped region corresponds to the Warburg resistance resulting from the frequency dependence of the ion diffusion/transport in the electrolyte. Again, GR/PT-50 and -67 showed a straight line closer to a 45°-sloped line, suggesting that these materials have better capacitive behaviour than PT. From the EIS analysis, it can be seen that GR/PT-50 showed a lower charge transfer resistance and a better capacitive behaviour than that of the PT. This result is consistent with the data shown in Figures 4 and 5. The reduced resistance of the composite probably arises from the network of the GR structure, which facilitates the efficient access of electrolyte ions to the surface and reduces the ion diffusion path. The GR/PT-50 composite has lower equivalent serial resistance, which is an important index for the ion diffusion rate from electrolyte to the surface of the electrode material. Based on the evidence presented above, GR/PT-50 is a promising material for applications as a supercapacitor.

4. CONCLUSIONS

In this study, traditional chemical polymerization was applied to synthesize a series of GR/PT composites with different mass percentage of PT: GR/PT-67, -50 and -33. The performance of each nanocomposite as supercapacitor was evaluated and compared. GR/PT-50 exhibited the best specific capacitance among the new materials (365 F g⁻¹ at 1 A g⁻¹) and also had a higher value than pure GR (232 F g⁻¹) and four times the value of the pure polymer PT (92 F g⁻¹). The high specific capacitance of this composite material gives it potential for use as an electrode material for supercapacitors. The improved electrical double-layer capacitance observed in the cyclic voltammetry experiments and the better rate capability of the GR/PT-50 composite compared to the other synthesized materials, might be due to the good pseudo-capacitance of the GR and a synergistic effect with the PT, which can shorten the ion diffusion length. The higher specific capacitance obtained for the GR/PT-50 composite when compared with that of GR can be ascribed to the rapid insertion/extraction of doping ions, a larger effective surface area and higher conductivity. Additionally, the introduction of the GR in a 1:1 proportion also showed an enhanced stability towards cycling. This stability makes the composite

material suitable for commercial applications, since a requirement for this is the possibility of using the material under different and varying working conditions throughout its shelf-life. In contrast, GR/PT-33 showed the worst capacitance conservation with an increase of the specific capacitance value of 54%, indicating that the material is destroyed with long cycling and thus it is not a good candidate for a supercapacitor because of its low capacity retention. This shows that a small variation in the composition can strongly influence the electrochemical behaviour as well as the material stability of the composite.

The impedance spectroscopy experiments showed that in the case of GR/PT-50 and -67, the electron transfer resistance is smaller. The incorporation of GR into the PT polymer in certain proportions seems to improve the conductive properties of the composite. GR/PT-50 and -67 also showed a straight line closer to vertical in the low frequency area of the Nyquist plot, suggesting that these materials have a behaviour closer to that of an ideal capacitor than the bare PT.

Based on our findings, the GR/PT-50 composite is a very promising material for applications as a supercapacitor.

ACKNOWLEDGEMENTS

This work was funded by Fondecyt Initiation Project N° 11140107. E.N.S is an assistant researcher of the Argentine National Council of Scientific and Technical Researches (CONICET). The work leading to this invention has received funding from the People Programme (Marie Curie Actions) of the European Union's Seventh Framework Programme (FP7/2007-2013) under REA grant agreement n° 629771.10.

References

1. D. Larcher and J.M. Tarascon, *Nat. Chem.*, 7 (2015) 19.
2. Z. Lin, Y. Liu, Y. Yao, O.J. Hildreth, Z. Li, K. Moon and C. Wong, *J. Phys. Chem. C*, 115 (2011) 7120.
3. H. Liu, J. Gao, M. Xue, N. Zhu, M. Zhang and T. Cao, *Langmuir*, 25 (2009) 12006.
4. T. Kuila, A.K. Mishra, P. Khanra, N.H. Kim, M.E. Uddin and J.H. Lee, *Langmuir*, 28 (2012) 9825.
5. D. Pech, M. Brunet, P.-L. Taberna, P. Simon, N. Fabre, F. Mesnilgrete, V. Conédéra and H. Durou, *J. Power Sources*, 195 (2010) 1266.
6. C. Liu, F. Li, L.P. Ma and H.M. Cheng, *Adv. Mater.*, 22 (2010).
7. B. Conway, *Electrochemical supercapacitor, Scientific Fundamentals and Technological Applications*, Springer US, 1999.
8. K.-W. Nam and K.-B. Kim, *J. Electrochem. Soc.*, 149 (2002) A346.
9. H.-Q. Wang, Z.-S. Li, Y.-G. Huang, Q.-Y. Li and X.-Y. Wang, *J. Mater. Chem.*, 20 (2010) 3883.
10. S.L. Candelaria, R. Chen, Y.-H. Jeong and G. Cao, *Energy Environ. Sci.*, 5 (2012) 5619.
11. Y. Sun, Q. Wu and G. Shi, *Energy Environ. Sci.*, 4 (2011) 1113.
12. Y. Cui, Q.-Y. Cheng, H. Wu, Z. Wei and B.-H. Han, *Nanoscale*, 5 (2013) 8367.
13. X. Wang and G. Shi, *Energy Environ. Sci.*, 8 (2015) 790.
14. M. Hughes, G.Z. Chen, M.S. Shaffer, D.J. Fray and A.H. Windle, *Chem. Mater.*, 14 (2002) 1610.
15. N. Levy, M.D. Levi, D. Aurbach, R. Demadrille and A. Pron, *J. Phys. Chem. C*, 114 (2010) 16823.
16. D. Dhawale, D. Dubal, V. Jamadade, R. Salunkhe and C. Lokhande, *Synth. Met.*, 160 (2010) 519.

17. K.A. Noh, D.-W. Kim, C.-S. Jin, K.-H. Shin, J.H. Kim and J.M. Ko, *J. Power Sources*, 124 (2003) 593.
18. A. Laforgue, P. Simon, C. Sarrazin and J.-F. Fauvarque, *J. Power Sources*, 80 (1999) 142.
19. H. Zhu, X. Wang, X. Liu and X. Yang, *Adv. Mater.*, 24 (2012) 6524.
20. X. Yang, C. Cheng, Y. Wang, L. Qiu and D. Li, *Science*, 341 (2013) 534.
21. P. Simon and Y. Gogotsi, *Nat. Mat.*, 7 (2008) 845.
22. Y. Zhu, S. Murali, M.D. Stoller, A. Velamakanni, R.D. Piner and R.S. Ruoff, *Carbon*, 48 (2010) 2118.
23. Y. Chen, X. Zhang, P. Yu and Y. Ma, *J. Power Sources*, 195 (2010) 3031.
24. X. Du, P. Guo, H. Song and X. Chen, *Electrochim. Acta*, 55 (2010) 4812.
25. J. Yan, T. Wei, B. Shao, Z. Fan, W. Qian, M. Zhang and F. Wei, *Carbon*, 48 (2010) 487.
26. Q. Wu, Y. Xu, Z. Yao, A. Liu and G. Shi, *ACS Nano*, 4 (2010) 1963.
27. X. Yan, J. Chen, J. Yang, Q. Xue and P. Miele, *ACS Appl. Mater. Interfaces.*, 2 (2010) 2521.
28. Y. Liu, H. Wang, J. Zhou, L. Bian, E. Zhu, J. Hai, J. Tang and W. Tang, *Electrochim. Acta*, 112 (2013) 44.
29. Y. Shao, M.F. El-Kady, L.J. Wang, Q. Zhang, Y. Li, H. Wang, M.F. Mousavi and R.B. Kaner, *Chem. Soc. Rev.*, 44 (2015) 3639.
30. M.R. Karim, C.J. Lee and M.S. Lee, *J. Polym. Sci., Part A: Polym. Chem.*, 44 (2006) 5283.
31. Q. Lu and Y. Zhou, *J. Power Sources*, 196 (2011) 4088.
32. J. Zhao, Y. Xie, Z. Le, J. Yu, Y. Gao, R. Zhong, Y. Qin and Y. Huang, *Synth. Met.*, 181 (2013) 110.
33. F. Alvi, M.K. Ram, P. Basnayaka, E. Stefanakos, Y. Goswami, A. Hoff and A. Kumar, *ECS Trans.*, 35 (2011) 167.
34. W.S. Hummers and R.E. Offeman, *J. Am. Chem. Soc.*, 80 (1958) 1339.
35. S. Stankovich, D.A. Dikin, R.D. Piner, K.A. Kohlhaas, A. Kleinhammes, Y. Jia, Y. Wu, S.T. Nguyen and R.S. Ruoff, *Carbon*, 45 (2007) 1558.
36. Y. Xu, H. Bai, G. Lu, C. Li and G. Shi, *J. Am. Chem. Soc.*, 130 (2008) 5856.
37. P. Khanra, C.-N. Lee, T. Kuila, N.H. Kim, M.J. Park and J.H. Lee, *Nanoscale*, 6 (2014) 4864.
38. D. Li, M.B. Mueller, S. Gilje, R.B. Kaner and G.G. Wallace, *Nat. Nanotech.*, 3 (2008) 101.
39. H.-K. Jeong, Y.P. Lee, R.J. Lahaye, M.-H. Park, K.H. An, I.J. Kim, C.-W. Yang, C.Y. Park, R.S. Ruoff and Y.H. Lee, *J. Am. Chem. Soc.*, 130 (2008) 1362.
40. A.B. Bourlinos, D. Gournis, D. Petridis, T. Szabó, A. Szeri and I. Dékány, *Langmuir*, 19 (2003) 6050.
41. C. Nethravathi, T. Nisha, N. Ravishankar, C. Shivakumara and M. Rajamathi, *Carbon*, 47 (2009) 2054.
42. S. Pan, X. Liu and X. Wang, *Mater. Charact.*, 62 (2011) 1094.
43. Z. Tang, L. Zhang, C. Zeng, T. Lin and B. Guo, *Soft Matter*, 8 (2012) 9214.
44. Y. Li, Q. Chen, K. Xu, T. Kaneko and R. Hatakeyama, *Chem. Eng. J.*, 215 (2013) 45.
45. B. Patil, A. Jagadale and C. Lokhande, *Synth. Met.*, 162 (2012) 1400.
46. E. Tahmasebi, Y. Yamini, M. Moradi and A. Esrafil, *Anal. Chim. Acta*, 770 (2013) 68.
47. O. Zabihi, A. Khodabandeh and S.M. Mostafavi, *Polym. Degrad. Stab.*, 97 (2012) 3.
48. X.-z. Guo, Y.-f. Kang, T.-l. Yang and S.-r. Wang, *T. Nonferr. Metal. Soc.*, 22 (2012) 380.
49. Y. Zhu, S. Xu, L. Jiang, K. Pan and Y. Dan, *React. Funct. Polym.*, 68 (2008) 1492.
50. M.R. Karim, K.T. Lim, C.J. Lee and M.S. Lee, *Synth. Met.*, 157 (2007) 1008.
51. M.G. Han and S.H. Foulger, *Adv. Mater.*, 16 (2004) 231.
52. S.R.P. Gnanakan, M. Rajasekhar and A. Subramania, *Int. J. Electrochem. Sci.*, 4 (2009) 1289.
53. X.-G. Li, J. Li, Q.-K. Meng and M.-R. Huang, *J. Phys. Chem. B*, 113 (2009) 9718.
54. J. Zhang, J. Ma, L.L. Zhang, P. Guo, J. Jiang and X.S. Zhao, *J. Phys. Chem. C*, 114 (2010) 13608.
55. J. Zhang, J. Jiang and X.S. Zhao, *J. Phys. Chem. C*, 115 (2011) 6448.
56. X. Yang, J. Zhu, L. Qiu and D. Li, *Adv. Mater.*, 23 (2011) 2833.
57. M. Wang, R. Jamal, Y. Wang, L. Yang, F. Liu and T. Abdiryim, *Nanoscale Res. Lett.*, 10 (2015) 1.

58. H.-P. Cong, X.-C. Ren, P. Wang and S.-H. Yu, *Energy. Environ. Sci.*, 6 (2013) 1185.
59. A. Alabadi, S. Razzaque, Z. Dong, W. Wang and B. Tan, *J. Power Sources*, 306 (2016) 241.
60. H. Nishihara and T. Kyotani, *Adv. Mater.*, 24 (2012) 4473.

© 2017 The Authors. Published by ESG (www.electrochemsci.org). This article is an open access article distributed under the terms and conditions of the Creative Commons Attribution license (<http://creativecommons.org/licenses/by/4.0/>).